JTTEE5 5:289-297

Corrosion Behavior of Ni-Cr Weld Overlay Alloys with Dispersed Carbide Particles in Sodium Chloride Solution

Y. Takatani, T. Tomita, K. Nagai, and Y. Harada

Ni-Cr weld overlay alloys with dispersed carbide particles were prepared by a plasma transferred arc welding process. The corrosion behavior of the 40 vol% carbide/Ni-Cr materials was studied in sodium chloride solution by electrochemical techniques, scanning electron microscopy, x-ray diffraction, and electron dispersive spectroscopy. The materials under investigation were powder blends of Ni-50 mass% Cr powder mixed with NbC, TaC, TiC, WC, Cr_3C_2, or VC. The NbC, TaC, TiC, and WC particles partially dissolved in the molten alloy, causing the crystallization of $M_{23}C_6$. Blends with Cr_3C_2 and VC particles produced the crystallization of M_7C_3, $V_xCr_yC_z$ and $M_{23}C_6$. The VC/Ni-Cr alloy combination caused preferential localized corrosion and the carbide remained as $V_xCr_yC_z$. The Cr_3C_2/Ni-Cr alloy combination became studded with the Cr-Cl corrosion product compound. With the WC/Ni-Cr alloy combination, the WC particles became oxidized and corrosion product spread over the matrix. Other carbides were not oxidized, but the matrix of the alloys with these dispersed particles did become covered with Cr-rich corrosion products. The NbC/Ni-Cr material exhibited the best corrosion resistance.

Keywords carbide particles, electrochemical measurement, nickel-chromium alloy, overlay weld alloy, plasma transferred arc welding process, sodium chloride

1. Introduction

TRANSITION-METAL carbides, in general, have high hardness, so a composite based on a corrosion-resistant alloy matrix containing such carbides should show good wear resistance as well as good corrosion resistance. A plasma transferred arc (PTA) welding method has been developed for coating steels with such composites (Ref 1), and the weldability (Ref 2, 3) and wear resistance (Ref 4) of these PTA coatings have been extensively examined.

After overlay welding with a blend of a nickel-chromium (Ni-Cr) alloy and various carbides by the PTA process, the welded alloy may consist of a Ni-Cr-*X* composition (where *X* is niobium, tantalum, titanium, tungsten, and vanadium) because these carbide particles (Ref 5, 6) go partially or totally into solution. There are many studies (Ref 7-13) about the influence of alloying elements o localized corrosion. The alloying elements chromium, niobium, and titanium improve the alloy corrosion resistance (Ref 9, 10), but tantalum and tungsten barely improve it (Ref 9), and vanadium has a tendency to increase the passive-current density (Ref 9).

In a previous study (Ref 14), the authors have shown the corrosion behavior of the transition-metal carbides in sodium chloride solution. WC and VC were anodically dissolved, and corrosion products of $WO_3/2H_2O$ and $V_2O_4/2H_2O$ were formed. Cr_3C_2 and TiC were stable in the passive region of corrosion potential and rapidly dissolved anodically in the transpassive region. The NbC and TaC particles were stable in sodium chloride solution.

It has been reported (Ref 15-18) that addition of a second phase such as carbide particles in metal causes crevice corrosion at the interface between the two phases, or galvanic corrosion between the carbide and the matrix alloy.

The purpose of this investigation is to clarify the effects of the carbide particles and matrix composition on the localized corrosion behavior of overlay alloys welded with dispersed carbide particles.

Y. Takatani, Hyogo Prefectural Institute of Industrial Research, Suma-Ku, Kobe, 654, Japan; **T. Tomita,** Hyogo Prefectural Institute of Industrial Research, Azafuke, Hirata, Miki, 673-04, Japan; and **K. Nagai** and **Y. Harada,** Tocalo Co., Ltd., Higashinada-Ku, Kobe, 658, Japan.

2. Experimental Procedure

2.1 *Preparation of Overlay Weld Alloys*

A Ni-50mass%Cr alloy powder (produced by Kobe Steel Co., Ltd., Wakinohama Chuo-Ku, Kobe, 651, Japan) and a carbide powder (purity: 99.9 mass%, produced by Nippon Sin Kinzoku Co., Ltd., Sennari Toyonaka-City, Osaka, 561, Japan) were used as starting materials. The particle size range of these powders was 60 to 150 μm. Figure 1 shows the morphology of the

Table 1 Chemical composition of the matrix on Ni-Cr overlay weld alloys with dispersed 40 vol% carbide particles determined by EDS

Alloy	Chemical composition, mass%			
	Ni	Cr	Fe	Other
Ni-Cr	50.0	46.8	3.2	
NbC/Ni-Cr	47.1	42.6	8.3	2.0 (Nb)
TiC/Ni-Cr	50.3	39 9	6 5	3.3 (Ti)
TaC/Ni-Cr	43.3	40.5	13.8	2.4 (Ta)
Cr_3C_2/Ni-Cr	45.9	50.4	3.7	
VC/Ni-Cr	50.3	28.8	12.5	8.4 (V)
WC/Ni-Cr	53.5	27.2	6.0	13.3 (W)

starting powders. The carbide materials were NbC, TaC, TiC, WC, Cr_3C_2, and VC. Ni-Cr alloy was mixed with 40 vol% carbide powder. Using these mixed powders, 4 mm thick Ni-Cr weld overlays with dispersed carbides were formed on mild steel (SS400, 150 by 150 by 25 mm) by the PTA process. Table 1 shows the chemical compositions of the matrix phases in the

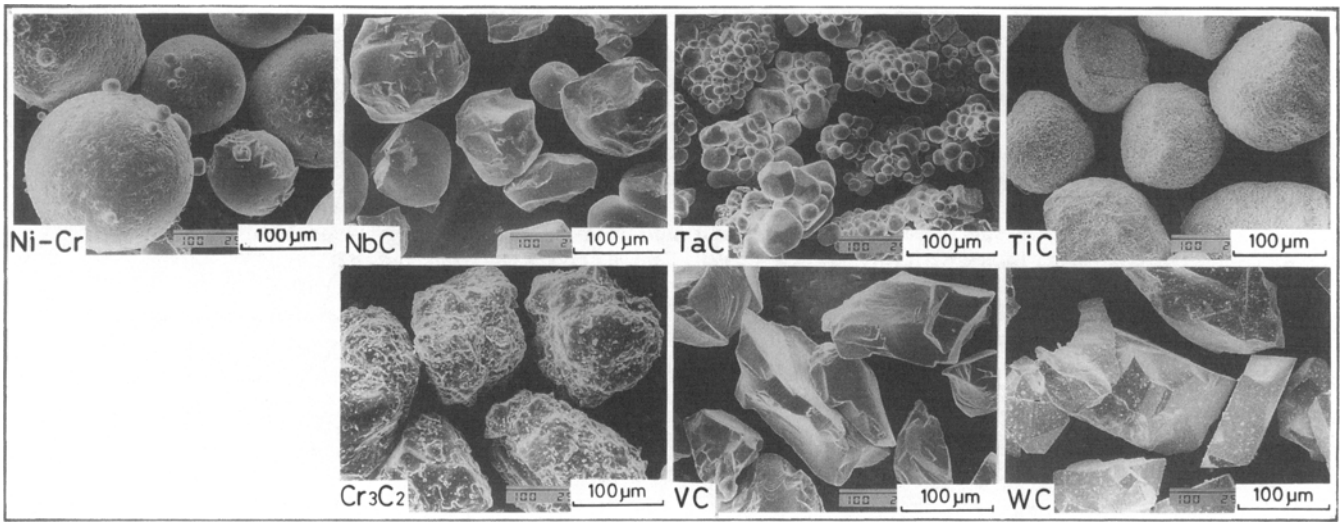

Fig. 1 Morphologies of Ni-Cr alloy and carbide particles

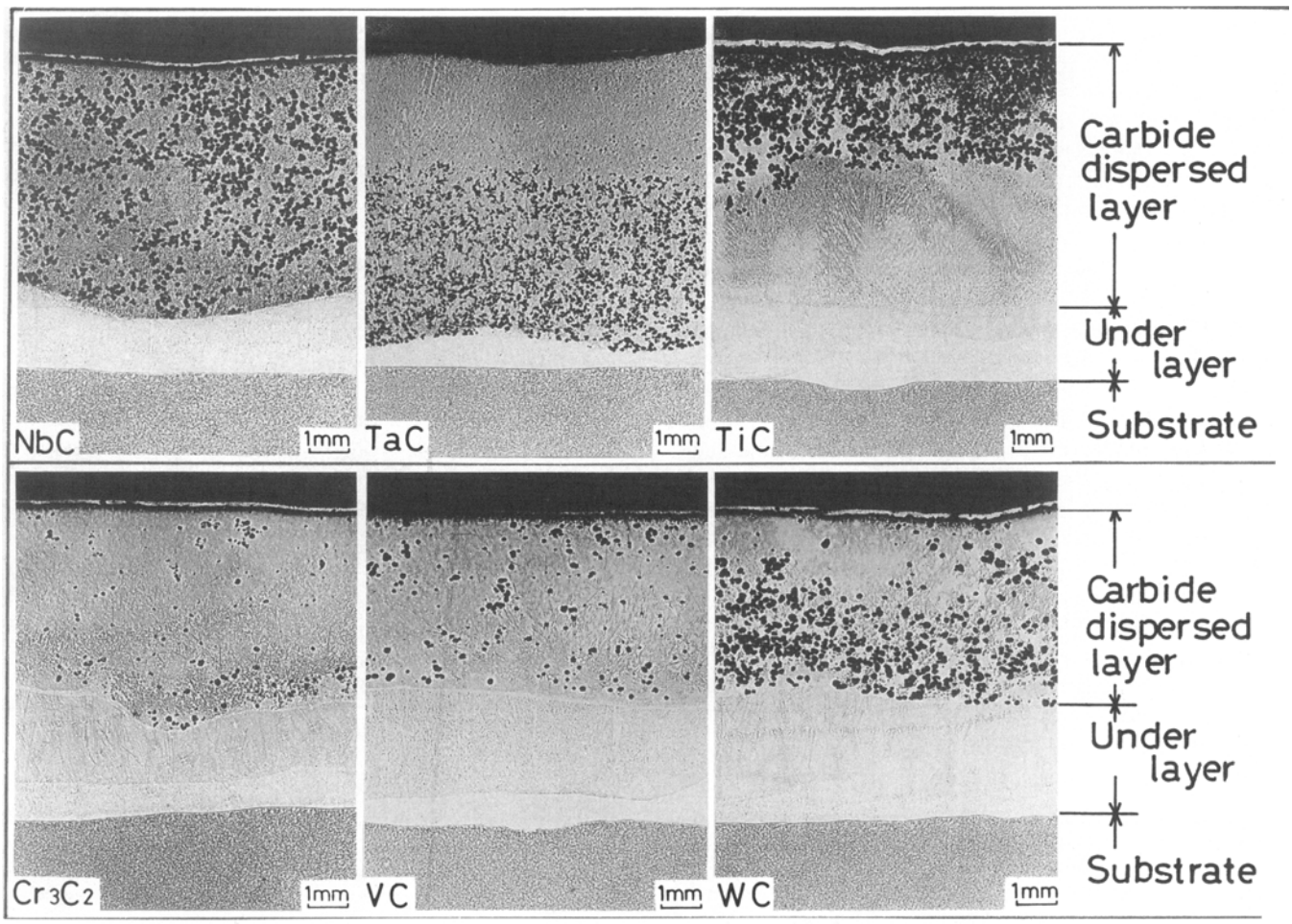

Fig. 2 Microstructures of cross section of the Ni-Cr weld overlay alloys with dispersed 40 vol% carbide particles

weld overlays, determined by electron dispersive spectroscopy (EDS) with a Phillips EDAX SW9100 (Phillips Electronic Instruments Co., Alpharetta, GA). Table 1 indicates that 3 to 13 mass% Fe is contained in the weld overlay.

A cross section of the overlay was polished using SiC papers and diamond paste. After electrolytic etching in a solution of 10 vol% HCl-90 vol% methyl alcohol, the microstructure of these alloys was examined by optical microscopy and scanning electron microscopy (SEM) (Hitachi Co., Ltd., Marunouchi Chiyoda-Ku, Tokyo, 100, Japan, S-800). The deposited carbides were identified by x-ray diffraction (XRD) (Rigakudenki Co., Ltd., Mathubara Akishima-City, Tokyo, 196, Japan, RAD-RC) using a monochromatic Cu-K_α x-ray source.

2.2 *Electrochemical Measurements*

For electrochemical polarization measurements, test specimens (15 by 15 mm) were cut from the weld overlay alloys. Copper wires were welded to the back of the specimen blocks, which were then mounted in epoxy. The electrode surface was polished with SiC papers up to No. 600 and rinsed with acetone. An electrode area of 10 by 10 mm was left by coating the rest of the surface with silicone resin.

Electrochemical testing was performed by means of potentiodynamic and potentiostatic polarization experiments. All electrochemical tests were conducted in 0.5 mol/L NaCl solution that was saturated by bubbling with air at least 3.6 ks before the polarization measurements and during the polarization run. An EG&G Princeton Applied Research (PAR) system was used in these tests (Model 273 potentiostat and Model 342 Programmer). All potential measurements were taken with respect to an Ag/AgCl/saturated KCl electrode. The counter electrode was platinum sheet. The temperature was kept at 323 K.

The surfaces of specimens were cleaned with demineralized water before immersion in the test solution. The potentiodynamic polarization testing was initiated at the corrosion potential when the specimen had been immersed in the solution for 0.6 ks. A scan of potential was carried out either in the electropositive direction at a rate of 0.2 mV/s until a breakdown potential was reached or in the electronegative direction to approximately –2.0 V with respect to Ag/AgCl at the same rate.

Potentiostatic polarization tests were also conducted on the weld overlay. At the pitting potential and at potentials anodic to the pitting potential in the same solution, the rising anodic current was recorded at 3.6 ks intervals by imposing potentiostatic control. After 3.6 ks, a positive potential up to 100 mV was set up.

2.3 *Analysis of Corrosion Surface*

The corrosion surfaces and pit morphologies of the weld overlay were observed after the anodic potentiostatic polarization tests. Scanning electron microscopy was used to examine the microstructure and corrosion morphology. Also, EDS was used for composition analysis of the overlay and its corrosion products. The corrosion product layers of specimens formed by potentiostatic polarization were washed with demineralized water, allowed to dry naturally, and placed in a dessicator before SEM and EDS examination.

3. Results and Discussion

3.1 *Morphology of Weld Overlay*

Optical microstructures of cross sections of the weld overlays with 40 vol% dispersed carbide particles are shown in Fig. 2. The white layer adjacent to the substrate is coated with melted

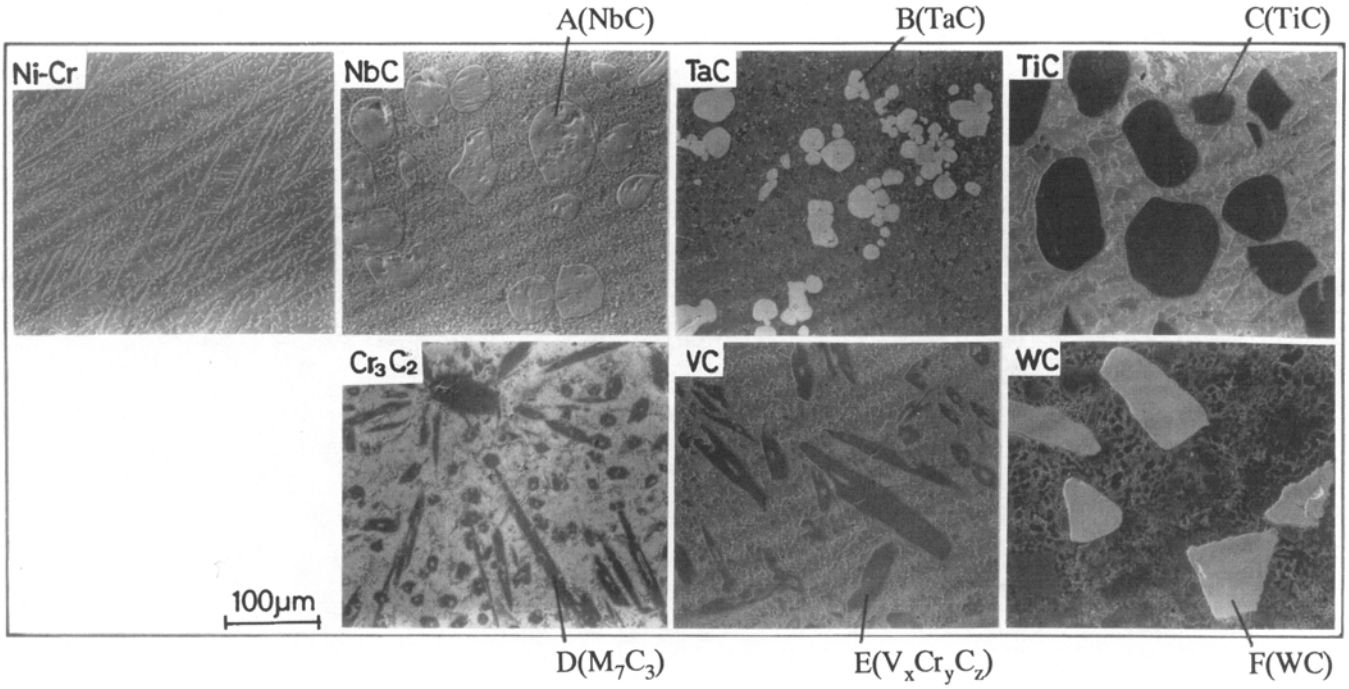

Fig. 3 Micrographs of the Ni-Cr weld overlay alloys with dispersed 40 vol% carbide particles

Ni-Cr powder. The upper layer, in which black particles are scattered, shows carbides dispersed in the Ni-Cr alloy. The NbC particle dispersion was almost uniform, but the TaC and WC particles were concentrated in the lower part of the layer, and the TiC particles in the upper part of the layer. Few Cr_3C_2 and VC particles remain visible, because these particles tend to go into solution during overlay welding by the PTA process. These layers have been examined by SEM. Their microstructures are shown in Fig. 3 and 4. The carbide-free Ni-Cr alloy shows a lamellar two-phase structure. Spherical particles (A, B, C, and F in Fig. 3) are the same as the black ones observed in Fig. 2, and these shapes are almost similar to the starting materials. It is suggested that only a thin layer of the surface of the starting particle has gone into solution, because these carbides have high melting points and the exposed time in the PTA process is very short.

For both the VC/Ni-Cr and Cr_3C_2/Ni-Cr alloy combinations, the microstructures of the deposits differ completely from those of the starting materials and the morphologies of the deposit are mainly columnar (E) or acicular (D). These carbides have low melting points and dissolve into the molten alloy during the PTA process and crystallize out at solidification. Additionally, Fig. 4 shows the details of the microstructures of the weld overlay shown in Fig. 3. It is indicated that dispersed carbides have polygonal (A and E), featherlike (G_1, G_2, G_3, and G_4), or islandlike (H_1, H_2, and H_3) structures.

The XRD measurements were carried out to identify deposited carbides. Figure 5 shows typical XRD patterns of the NbC/Ni-Cr alloy combination, in which γ-phase, α-phase, NbC, and $M_{23}C_6$ are detected. The XRD results are summarized in Table 2.

Table 2 confirms that the deposited carbides in the alloy are crystallized NbC, TiC, M_7C_3, $V_xCr_yC_z$, M_6C, and $M_{23}C_6$, plus any unmelted carbide particles. The carbide-free Ni-Cr alloy is composed of γ- and α-phases with a lamellar structure (Ref 5). The polygonal deposit (A) in the NbC/Ni-Cr overlay is NbC compound. The columnar and polygonal deposits (E) in the VC/Ni-Cr overlay are $V_xCr_yC_z$. The acicular phases (D) in the Cr_3C_2/Ni-Cr overlay are M_7C_3. The featherlike phases (G) shown in all the micrographs in Fig. 4 are $M_{23}C_6$. Furthermore the island-like phases (H_1 and H_2) can be regarded as the α-phase. The deposit (H_3) in the Cr_3C_2/Ni-Cr overlay is a mixture of γ-phase and chromium carbide.

3.2 *Polarization Behavior*

The potentiodynamic polarization curves for the weld overlays with 40 vol% dispersed carbides in aerated 0.5 *M* NaCl solution at 323 K are shown in Fig. 6. The corrosion potential of all alloys is around –0.2 V versus Ag/AgCl. Cathodic polarization curves of carbide-free Ni-Cr and NbC/Ni-Cr materials show a linear current rise. Cathodic currents of the TiC/Ni-Cr, the TaC/Ni-Cr, the Cr_3C_2/Ni-Cr, the VC/Ni-Cr, and the WC/Ni-Cr materials rise slowly, and then linearly. For the materials with NbC, TiC, VC particles, or particles without carbides, anodic polarization curves show a constant current region between the corrosion potential and breakdown potential. A wide range of breakdown potentials are evident for the NbC/Ni-Cr alloy. The pitting potential is the most electropositive for the carbide-free Ni-Cr and the VC/Cr-Ni overlays. Therefore, the dispersion of the NbC in the Ni-Cr alloy is seen to improve pitting corrosion resistance. For the TiC/Ni-Cr, the TaC/Ni-Cr, and the WC/Ni-Cr materials, the anodic current linearly increases as potential increases from the corrosion potential. Only for the Cr_3C_2/Ni-Cr overlay, is there an active-dissolution peak at –0.2 V, and a rapid increase in current.

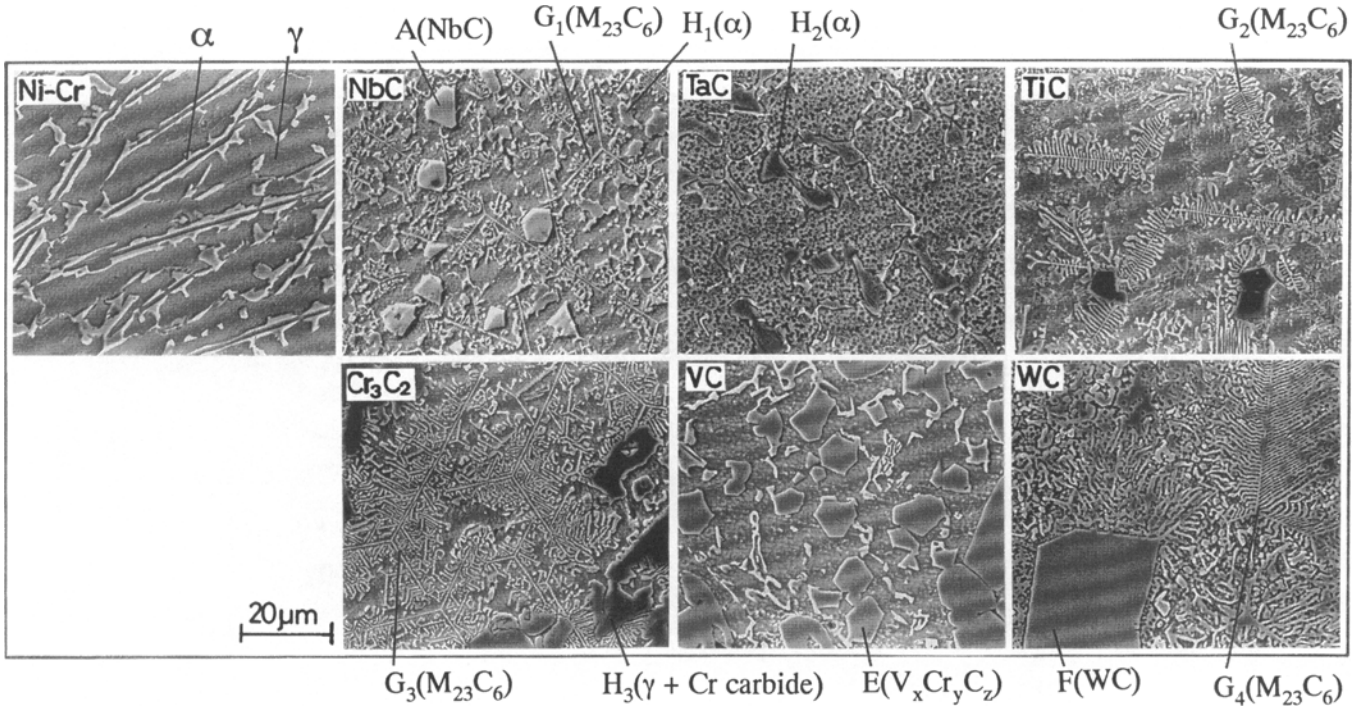

Fig. 4 Microstructures of the Ni-Cr weld overlay alloy with dispersed 40 vol% carbide particles in Fig. 3

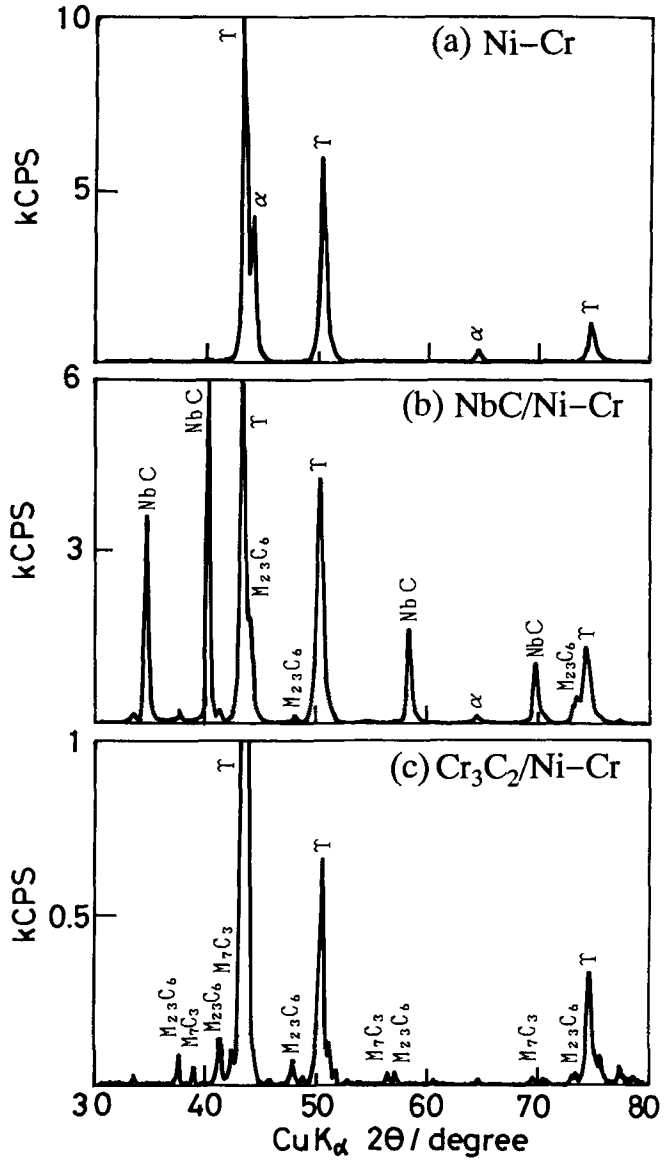

Fig. 5 X-ray diffraction patterns of the Ni-Cr weld overlay alloy with dispersed 40 vol% carbide particles. (a) Carbide-free. (b) NbC. (c) Cr_3C_2

Table 2 The carbides and the matrix phases of Ni-Cr overlay weld alloys with 40 vol% carbide particles determined by XRD and EDS

Alloy	Unmelted carbide	Crystallized carbides	Matrix phases
Ni-Cr			γ, α
NbC/Ni-Cr	NbC	NbC, $M_{23}C_6$	γ, α
TiC/Ni-Cr	TiC	TiC, $M_{23}C_6$	γ, α
TaC/Ni-Cr	TaC	$M_{23}C_6$	γ, α
Cr_3C_2/Ni-Cr		M_7C_3, $M_{23}C_6$	γ
VC/Ni-Cr		$V_xCr_yC_z$, $M_{23}C_6$	γ
WC/Ni-Cr	WC	M_6C, $M_{23}C_6$	γ

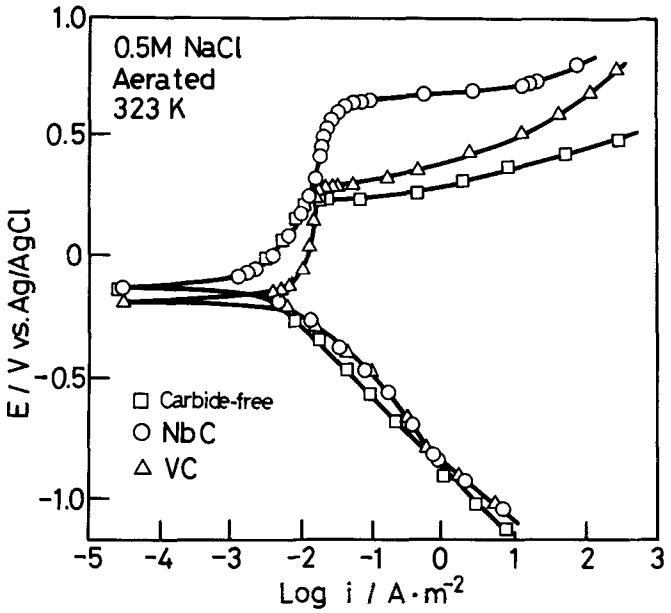

(a)

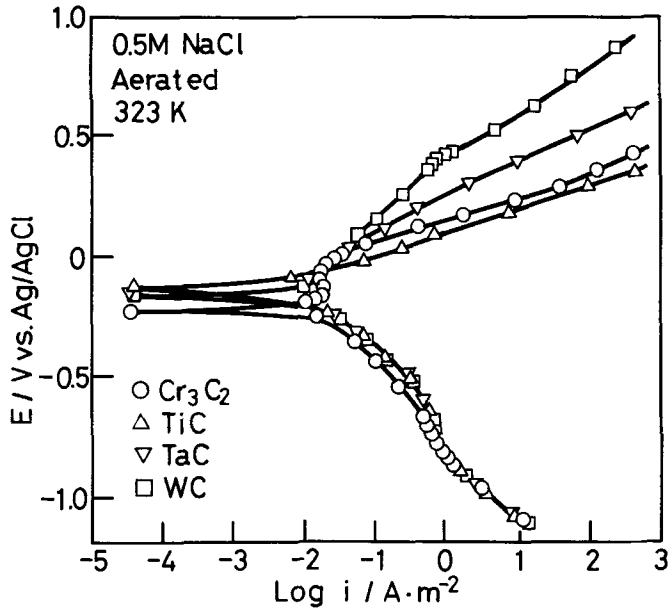

(b)

Fig. 6 Polarization curves of the Ni-Cr weld overlay alloys with dispersed 40 vol% carbide particles in aerated 0.5 mol/L NaCl solution at 323 K. (a) Carbide-free, NbC, and VC. (b) Cr_3C_2, TiC, TaC, and WC

The potentiostatic tests of the alloys are performed while holding at various potentials. Figure 7 shows the changes in anodic current density, which were monitored over 1 h. At low potentials, before the current rises, the currents of the carbide-free Ni-Cr (Fig. 7a) and the NbC/Ni-Cr (Fig. 7b) overlays are constant, yet most electronegative values for the carbide-free Ni-Cr alloy is identical. Currents of the WC/Ni-Cr (Fig. 7c) and the VC/Ni-Cr (Fig. 7d) materials increase as the potential increases. The results of the TiC/Ni-Cr and the Cr_3C_2/Ni-Cr materials show the same tendency as those of the WC/Ni-Cr alloy, though this is not shown in Fig. 7.

3.3 *Corrosion Surface*

Figure 8 shows SEM micrographs of the alloy surface after polarization in aerated 0.5 mol/L NaCl solution at potentials up to the breakdown potential for 3.6 ks, as shown in Fig. 7. It can be seen that the carbide-free Ni-Cr (Fig. 8a) and the VC/Ni-Cr

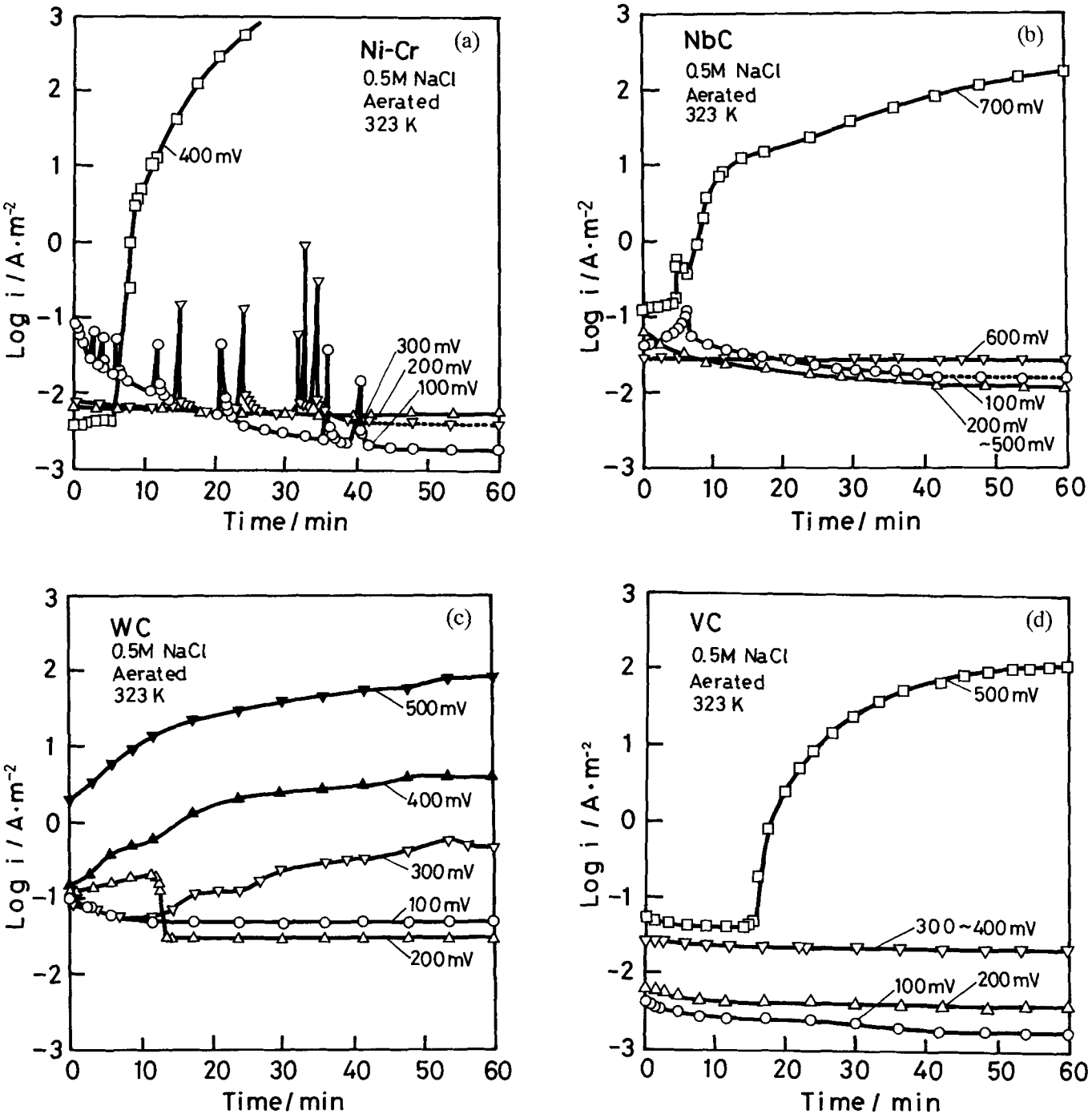

Fig. 7 Variation of current densities during the potentiostatic polarization of the Ni-Cr weld overlay alloys with dispersed 40 vol% carbide particles in aerated 0 5 mol/L NaCl solution at 323 K. (a) Carbide-free. (b) NbC (c) WC. (d) VC

(Fig. 8f) alloys show pits, the NbC/Ni-Cr (Fig. 8b), TaC/Ni-Cr (Fig. 8c), TiC/Ni-Cr (Fig. 8d), and WC/Ni-Cr (Fig. 8g) alloys have films over the matrix surfaces, and the Cr_3C_2 (Fig. 8e)/Ni-Cr is studied with a white deposit. Also, in the WC/Ni-Cr deposits, localized white protuberances are observed. Figure 9 shows the details of these pits observed in Fig. 8. In Fig. 9(a), a pit in the carbide-free Ni-Cr deposit is shown to have resulted from selective dissolution of the Ni-rich γ-phase out of the lamellar chromium-rich α-phase, as reported previously (Ref 6). Figure 9(b) shows a pit for the VC/Ni-Cr after the matrix alloy dissolved and $V_xCr_yC_z$ remained, where EDS analysis indicated a V-Cr compound. The protuberance in Fig. 8(g) is an oxidation product WC, $WO_3/2H_2O$ (Ref 14, 19). Figure 10 shows the SEM microstructure and the EDS profiles of corrosion product films on the NbC/Ni-Cr, the TiC/Ni-Cr, the WC/Ni-Cr, and TaC/Ni-Cr deposits. It seems that all the corrosion product films covering the matrix surface are chromium-rich compounds containing only a small amount of nickel when compared with the EDS profiles of the starting material in Fig. 11. The studded materials shown in Fig. 8(e) for the Cr_3C_2/Ni-Cr alloy are corrosion products that are rich in Cr-Cl compounds as indicated by the EDS analysis (Fig. 11).

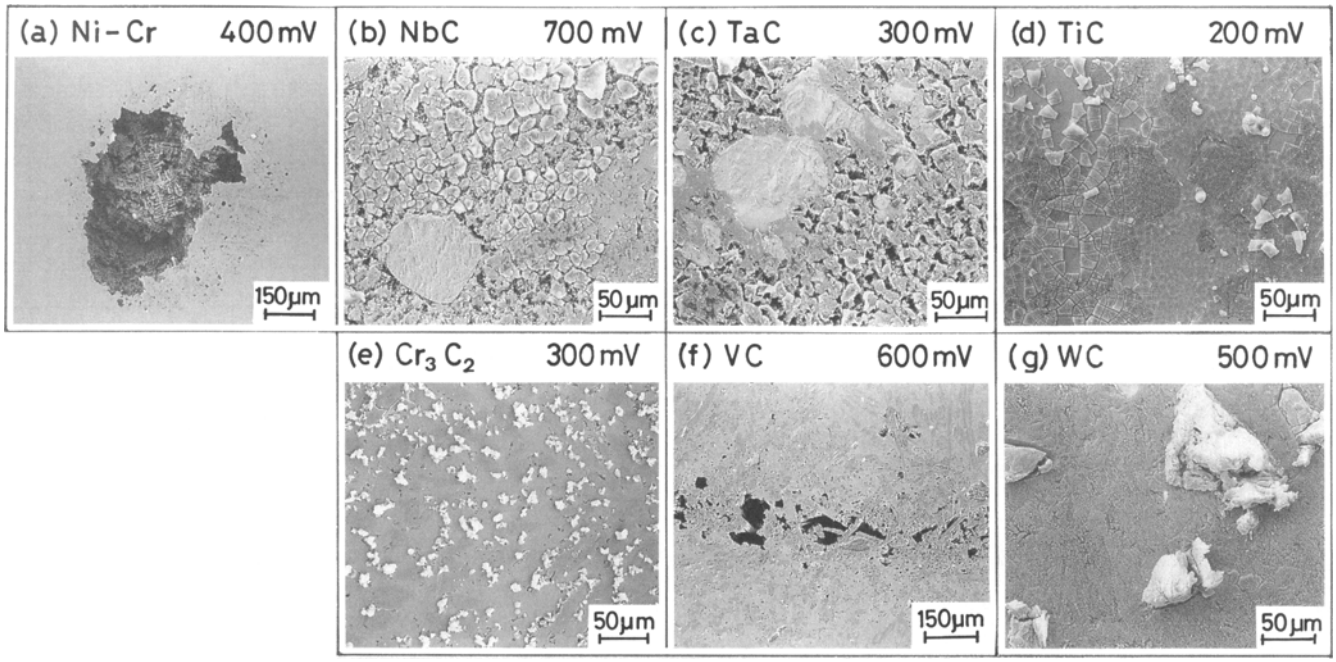

Fig. 8 SEM micrographs of the Ni-Cr weld overlay alloys with dispersed 40 vol% carbide particles after the potentiostatic polarization in aerated 0.5 mol/L NaCl solution at 323 K. Carbide and potential (versus Ag/AgCl): (a) Carbide-free at 400 mV. (b) NbC at 700 mV. (c) TaC at 300 mV. (d) TiC at 200 mV. (e) Cr_3C_2 at 300 mV. (f) VC at 600 mV. (g) WC at 500 mV

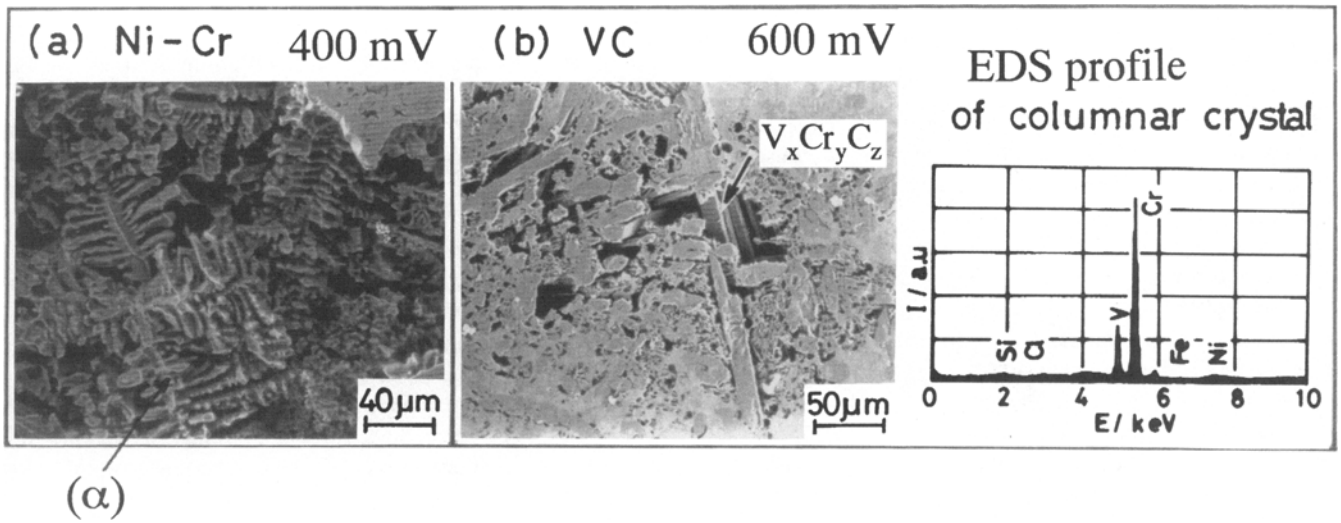

Fig. 9 SEM micrographs of the localized corrosion for the Ni-Cr weld overlay alloys without and the dispersed 40 vol% VC particles and EDS profile of remnant particles of the latter alloys (shown in Fig. 8a and f)

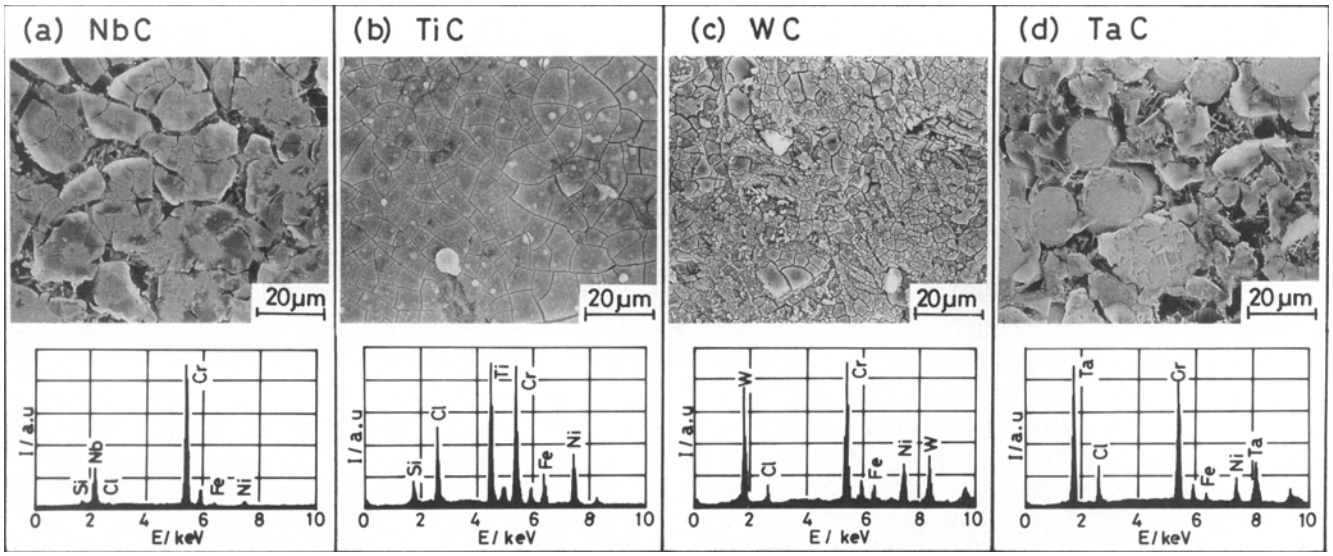

Fig. 10 SEM micrographs and EDS profiles of corrosion products of the Ni-Cr weld overlay alloys with dispersed 40 vol% carbide particles shown in Fig. 8. (a) NbC. (b) TiC. (c) WC. (d) TaC

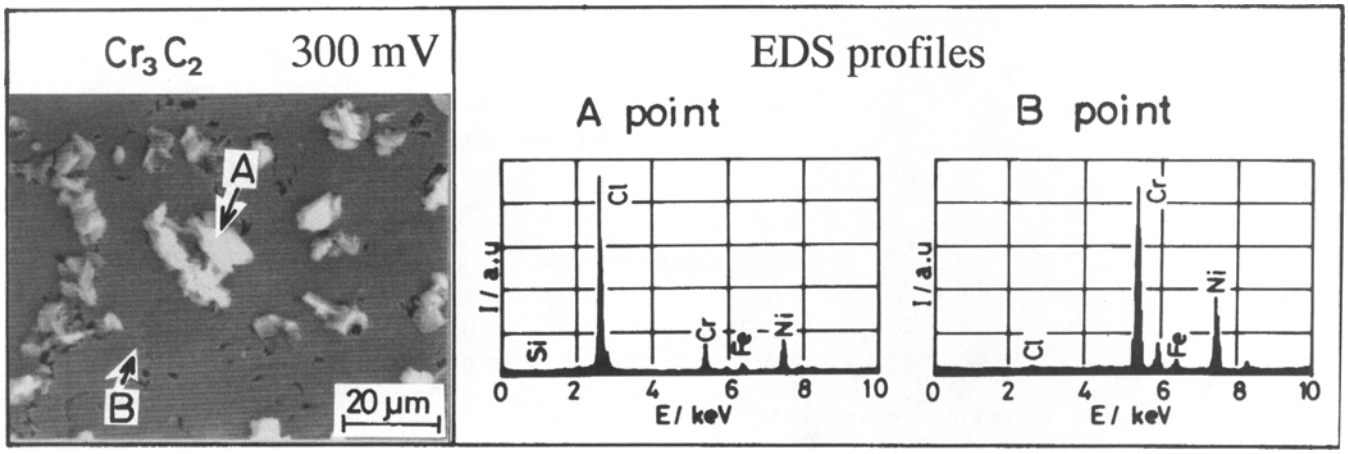

Fig. 11 SEM micrograph and EDS profiles of corrosion products of the Ni-Cr weld overlay alloys with dispersed 40 vol% Cr_3C_2 particles shown in Fig. 8(e)

3.4 *Corrosion Behavior*

Although the Ni-Cr powders are used in the PTA process (Ref 5, 6), the weld overlay has a Ni-Cr-Fe matrix because iron enters from the steel substrate. In this study, the alloys had iron contents ranging from 3 to 13 mass%. The pitting resistance of such an alloy in neutral chloride solution is dependent on the matrix composition.

The pitting resistance increases considerably for chromium contents greater than 30 mass% (Ref 10, 11). When nickel and chromium are present together, the pitting potential shifts rapidly to the noble side as the nickel content rises to 13 mass% (Ref 12), but the rise of potential is only 0.1 V between 15 and 60 mass% Ni (Ref 10). The pitting potential for the Ni-Cr alloy free of carbides and containing only 3 mass% Fe remained at 0.4 V in spite of the 50 mass% Cr, so the pitting resistance was poor in spite of low iron. A nickel-rich phase of the carbide-free Ni-Cr alloy is ascribed to preferential dissolution, as shown in Fig. 7(a), arising from inhomogeneity.

Furthermore, the matrix of the weld overlay alloys may consist of a Ni-Cr-Fe-*X* composition (where *X* is niobium, tantalum, titanium, tungsten, and vanadium) as shown in Table 1, because of dissolution of the carbide particle surface or of complete particles in the PTA process.

It is well known that transition metals such as chromium, nickel, and niobium enhance the corrosion resistance of stainless steels. The pitting potential for the NbC/Ni-Cr alloy shifted to the most noble side in all alloys. There is no pitting even in the transpassive region. Anodic polarization at 1.0 V produces a Cr-Nb-rich film covering the surface. Thus, alloying with niobium would give high corrosion resistance in sodium chloride solution.

The corrosion behavior of the TaC/Ni-Cr material is considered to be similar to that of the NbC/Ni-Cr material according to

the corrosion morphologies shown in Fig. 8 and 10. But, the anodic polarization curve of the TaC/Ni-Cr material shows an anodic dissolution current that is different from that of the NbC/Ni-Cr alloy. As a result, the tantalum alloying element in the Ni-Cr alloy does not exhibit any affect. Whereas the TiC/Ni-Cr alloy shows an increase in anodic current from a low potential at –0.2 V, the matrix surface is covered with a corrosion product film and there is no localized corrosion.

In the Cr_3C_2/Ni-Cr material, the Cr_3C_2 particles transform themselves into M_7C_3 and $M_{23}C_6$, the matrix phase surface is not covered with the corrosion product film, and its products are studded on the surface. The anodic dissolution occurs rapidly. It cannot be shown whether both M_7C_3 and matrix alloy dissolve because the matrix contains the same element as the carbide particle. However, the nickel element of the matrix is found in the solution; therefore, the dissolution of the matrix alloy in the Cr_3C_2/Ni-Cr material occurs.

The carbides such as VC and WC were oxidized in sodium chloride solution (Ref 14). On dispersing the VC particle in this Ni-Cr alloy by the PTA process, the VC deposits as $V_xCr_yC_z$ and the matrix alloy is reduced to a Ni-Cr-V composition. The pitting shows the same corrosion morphology as the carbide-free Ni-Cr alloy. The WC/Ni-Cr alloy would be oxidized by both the matrix and WC particle, which changes to a W-oxide, probably to a compound of WO_3/H_2O (Ref 19).

Hence, it has become apparent that the carbide/Ni-Cr materials have four kinds of corrosion behavior. In the NbC/Ni-Cr alloy, the matrix alloy has high corrosion resistance and carbide particles do not dissolve. The carbide-free Ni-Cr and the VC/Ni-Cr alloys with matrix cause selective dissolution. The corrosion products deposit over the surface of the matrix alloy, and these carbides are oxidized. Both carbide particles and the matrix alloy are oxidized.

4. Conclusions

The corrosion behavior of the Ni-Cr weld overlay alloys with dispersed carbide particles prepared by the plasma transferred arc method was studied in sodium chloride solution. Partial solution of NbC, TaC, TiC, and WC particles dissolved in molten alloy caused the crystallization of $M_{23}C_6$. Particles of Cr_3C_2 and VC produced the crystallization of M_7C_3, $V_xCr_yC_z$, and $M_{23}C_6$. The VC/Ni-Cr alloy caused selective corrosion. The Cr_3C_2/Ni-Cr alloy was studded with the Cr-Cl corrosion product compound. The WC/Ni-Cr alloy caused the WC particle to be oxidized, and corrosion product covered the matrix surface. Other carbides were not oxidized and the matrix of the alloys with dispersed carbide particles was covered with chromium-rich corrosion products. The NbC/Ni-Cr material exhibited the best corrosion resistance.

Acknowledgments

The authors thank Prof. Harushige Tsubakino of Himeji Institute of Technology for helpful discussions.

References

1. M. Nakajima, M. Ueda, and T. Nohtomi, Formation of Carbide Dispersion Type Overlay Weld by Plasma Arc, *J. Jpn. Weld. Soc.*, Vol 50 (No. 5), 1981, p 471-477
2. T. Kato and Y. Takeuchi, Present Condition of Hardfacing by Plasma Arc with Powder Fillers, *J. Iron Steel Inst. Japan*, Vol 75 (No. 1), 1989, p 42-49
3. T. Tomita,, Y. Takatani, and Y Harada, Alloying of Metal Surface by Plasma Transferred Arc Welding Process, *Mater. Jpn.*, Vol 31 (No. 12), 1992, p 1056-1063
4. T. Tomita, Y. Takatani, G. Hashizume, and Y. Harada, Microstructure and Wear Property of Ni-Cr Overlay Weld Alloy with Dispersed Various Carbide Particles, *J. High Temp. Soc.*, Vol 20 (No. 5), 1994, p 208-218
5. T. Tomita, Y. Takatani, G. Hashizume, and Y. Harada, Solidification Process of Ni-Cr-Fe Overlay Weld Alloy with Dispersed NbC Particles, *Mater. Trans.*, JIM, Vol 34 (No. 1), 1993, p 69-75
6. Y. Takatani, T. Tomita, G. Hashizume, and Y. Harada, Localized Corrosion of Ni-Cr-Fe Overlay Weld Alloys with Dispersed NbC in Sodium Chloride Solution, *Boshoku Gijutsu (Corros. Eng.)*, Vol 38 (No. 8), 1989, p 422-428
7. S. Szklarska Smialowska, *Localized Corrosion: Iron-Chromium-Nickel Alloy*, B.F. Brown, J. Kruger, and R.W. Staele, Ed.,, National Association of Corrosion Engineers, 1974, p 314
8. M. Kowaka, *Metallic Corrosion Damage and Protection*, Agune, Tokyo, 1983, p 301
9. N.D. Tomashov, G.P. Tchernova, and O.N. Marcova, Effect of Supplementary Alloying Elements on Pitting Susceptibility of 18Cr-14Ni Stainless Steel, *Corrosion*, Vol 20, May 1964, p 166t-173t
10. J. Horvath and H.H. Uhlig, Critical Potentials for Pitting Corrosion of Ni, Cr-Ni, Cr-Fe, and Related Stainless Steels, *J. Electrochem. Soc.*, Vol 115 (No. 8), 1968, p 791-795
11. R.F. Steigerwald, Effect of Cr Content on Pitting Behavior of Fe-Cr Alloys, *Corrosion*, Vol 22, April 1966, p 107-112
12. A.M. Kolotyrkin, Pitting Corrosion of Metals, *Corrosion*, Vol 19, Aug 1963, p 261t-268t
13. F.G. Hodge and B.E. Wilde, Effect of Chloride Ion on the Anodic Dissolution Kinetics of Chromium-Nickel Binary Alloys in Dilute Sulfuric Acid, *Corrosion*, Vol 26 (No. 6), 1970, p 146-150
14. Y. Takatani, T. Tomita,, and Y. Harada, Corrosion Behavior of Carbides in Sodium Chloride Solution, *J. Soc. Mater. Sci., Jpn.*, Vol 41 (No. 468), 1989, p 1348-1353
15. H. Sun, E.Y. Koo, and H.G. Wheat, Corrosion Behavior of SiCp/6061 Al Metal Matrix Composites, *Corrosion*, Vol 47 (No. 10), 1991, p 741-753
16. P.P. Trzaskoma, E. McCafferty, and C.R. Crowe, Corrosion Behavior of SiC/Al Metal Matrix Composites, *J. Electrochem. Soc.*, Vol 130 (No. 9), 1983, p 1804-1809
17. D.M Aylor and P.J. Moran, Effect of Reinforcement on the Pitting Behavior of Aluminum-Base Metal Matrix Composites, *J. Electrochem. Soc.*, Vol 132 (No. 6), 1985, p 1277-1281
18. I. Dutta, L.R. Elkin, and J.D. King, Corrosion Behavior of a P130x Graphite Fiber Reinforced 6063 Aluminum Composite Laminate in Aqueous Environments, *J. Electrochem. Soc.*, Vol 138 (No. 11), 1991, p 3199-3209
19. H. Nakahira, Y. Harada, T. Doi, Y Takatani, and T. Tomita, The Corrosion Resistance of High Velocity Flame Sprayed WC Cermet Coatings, *J. High Temp. Soc., Jpn.*, Vol 16, 1990, p 317-324